

High-Performance Magnesium-Sulfur Batteries Based on a Sulfurated Poly(acrylonitrile) Cathode, a Borohydride Electrolyte, and a High-Surface Area Magnesium Anode

Peiwen Wang^{+, [a]}, Janina Trück^{+, [a, c]}, Stefan Niesen^{+, [a, c]}, Julian Kappler^{+, [a]}, Kathrin Küster^{+, [d]}, Ulrich Starke^{+, [d]}, Felix Ziegler^{+, [a]}, Andreas Hintennach^{+, [c]} and Michael R. Buchmeiser^{+, [a, b]}

Post-lithium-ion battery technology is considered a key element of future energy storage and management. Apart from high gravimetric and volumetric energy densities, economic, ecologic and safety issues become increasingly important. In that regards, both the anode and cathode materials must be easily available, recyclable, non-toxic and safe, which renders magnesium-sulfur (Mg–S) batteries a promising choice. Herein, we present Mg–S cells based on a sulfurated poly(acrylonitrile) composite cathode (SPAN), together with a halogen-free electrolyte containing both Mg[BH₄]₂ and Li[BH₄] in diglyme and

a high-specific surface area magnesium anode based on Rieke magnesium powder. These cells deliver discharge capacities of 1400 and 800 mAh/g_{sulfur} with >99% Coulombic efficiency at 0.1 C and 0.5 C, respectively, and are stable over at least 300 cycles. Energy densities are 470 and 400 Wh/kg_{sulfur} at 0.1 C and 0.5 C, respectively. Rate tests carried out between 0.1 C and 2 C demonstrate good rate capability of the cells. Detailed mechanistic studies based on X-ray photoelectron spectroscopy and electric impedance spectroscopy are presented.

1. Introduction

There is a growing demand for efficient energy storage materials in the era of post-lithium-ion battery technology. Because of the high theoretical energy density of both, sulfur and magnesium,^[1–2] rechargeable magnesium sulfur (Mg–S) batteries are attractive candidates. At the same time, magnesium is considered a safer choice in commercial applications due to its predominantly non-dendritic plating.^[3] However, compared to Li–S batteries, the accomplishments in the field of Mg–S batteries are still quite limited, mainly due to the lack of suitable electrolytes that improve the sluggish kinetics of the bivalent Mg²⁺ ions and the poor plating performance of Mg anodes.^[2]

Most cathode materials for Mg–S batteries reported so far accommodate the sulfur in different porous and highly

conductive carbon materials, such as carbon black,^[1] CMK-3,^[4–6] nitrogen-doped graphene,^[7] carbon nanotubes,^[8] carbon nanofibers,^[9–10] activated carbon cloths^[11–12] or reduced graphene oxide.^[13] General important features of these cathode materials are that they possess good electrical conductivity, impede the polysulfide diffusion and show high mechanical stability.^[13]

Anodes for Mg–S cells are mostly based on low specific surface area Mg foils. Upon contact with traces of oxygen or air, however, Mg immediately forms a passivating layer (approximately 10 nm) containing oxides, carbonates and hydroxides.^[11,14–17] To remove the passivation layer and to activate the Mg, the foils are usually scratched under an inert atmosphere. However, this approach is of limited reproducibility and hard to scale.

Currently used electrolytes comprise Al-, B- or Y-based Lewis acids together with a magnesium-derived Lewis base, such as Mg bis(hexamethyldisilazide), Mg[HMDs]₂, prepared via a transmetalation reaction.^[8,18–19] Complementary, the use of magnesium salts containing a weakly coordinating anion such as Mg bis(tetrakis(hexafluoropropoxyborate)), Mg[B(hfip)₄]₂, has also been outlined.^[6,20] Unfortunately, with this type of salt, capacity fading has been observed.^[20] Finally, the addition of some lithium salts, e.g. lithium bis(trifluoromethylsulfon)imide, LiTFSI, and LiCl, to a magnesium salt-containing electrolyte has been reported to result in improved reversibility and discharge capacities.^[4,11,21–22]

Here, we present a halogen-free dual salt electrolyte system based on Mg[BH₄]₂ and Li[BH₄] together with an alternative active cathode materials based on a sulfur-carbon composites, e.g., sulfur-poly(acrylonitrile) (“SPAN”).^[23–26] In SPAN, the sulfur is not physisorbed but chemically bound to the carbonaceous backbone, predominantly as vinylogous/phenylogous enolic


[a] P. Wang,⁺ J. Trück,⁺ S. Niesen, J. Kappler, F. Ziegler, Prof. M. R. Buchmeiser
 Institute of Polymer Chemistry, University of Stuttgart
 Pfaffenwaldring 55, 70569 Stuttgart, Germany
 E-mail: michael.buchmeiser@ipoc.uni-stuttgart.de


[b] Prof. M. R. Buchmeiser
 German Institutes of Textile and Fiber Research (DITF) Denkendorf
 Körschtalstraße 26, 73770 Denkendorf, Germany

[c] J. Trück,⁺ S. Niesen, Prof. A. Hintennach
 Daimler AG, RD/EBT
 Hanns-Klemm-Straße 45, 71034 Böblingen, Germany

[d] K. Küster, Prof. U. Starke
 Max Planck Institute for Solid State Research
 Heisenbergstraße 1, 70569 Stuttgart, Germany

[*] These authors contributed equally to this work.

 Supporting information for this article is available on the WWW under <https://doi.org/10.1002/batt.202000097>

 © 2020 The Authors. Published by Wiley-VCH Verlag GmbH & Co. KGaA. This is an open access article under the terms of the Creative Commons Attribution License, which permits use, distribution and reproduction in any medium, provided the original work is properly cited.

thioamides, which allows for the formation of intra- and intermolecular polymer- S_x -polymer chains ($2 \leq x \leq 8$). The thioamide bond in its enolate form distinguishes SPAN from most other S-based cathodes. We also present a novel approach to high specific surface area Mg anodes. It comprises the synthesis of Rieke Mg powder via the reduction of magnesium chloride under inert atmosphere.^[27] Its particle size is in the sub-micrometer range resulting in a comparably large specific surface area.

2. Results and Discussion

Because of the divalent nature of the Mg^{2+} cation, ion pair formation with the oligosulfides, S_x^{2-} ($1 \leq x \leq 8$), that form during discharge results in different oligomeric structures ($S_x^{2-}Mg^{2+}$)_{*n*} ($n \geq 1$). Their solubility strongly depends on the solvent used. Also, the predominantly non-dendritic plating of Mg imposes a challenge.^[3] While this is highly beneficial in terms of battery safety, it results in a comparably low specific surface area of the anode and limited formation of fresh Mg surface during charging. Together with its pronounced ability to form an oxide/hydroxide-based passivation layer, Mg-S batteries suffer from poor cycle stability and very limited rate capability.^[2]

2.1. Electrolyte

One way to remove Mg hydroxide/oxide layers is the use of hydrides, e.g. $Mg[BH_4]_2$. Unfortunately, the solubility of $Mg[BH_4]_2$ is only 0.01 M in diglyme.^[28] However, with the addition of $Li[BH_4]$, its solubility increases to 0.1 M. Moreover, due to the mediating role of Li^+ , its presence can be expected to promote the formation of mixed cation, i.e. of Li^+/Mg^{2+} (poly)sulfides. Previous research demonstrated that this type of electrolyte is electroactive, but performs poorly with standard sulfur-containing carbonaceous materials.^[28] However, in view of the excellent long-time cycle stability of Li-SPAN cells with an LiTFSI/ether-based electrolyte,^[24,29] a SPAN-based cathode material was chosen and expected to display a similar performance in Mg-S cells using this Mg^{2+}/Li^+ hybrid electrolyte.

The influence of the concentration of the Li salt on cycle performance was studied using three different electrolyte systems: (i) 0.1 M $Mg[BH_4]_2/0.5$ M $Li[BH_4]$, (ii) 0.1 M $Mg[BH_4]_2/1$ M $Li[BH_4]$ and (iii) 0.1 M $Mg[BH_4]_2/1.5$ M $Li[BH_4]$. Diglyme was chosen as solvent due to its high dielectric constant ($\epsilon = 7.23$ at 298 K) compared to 1,2-dimethoxyethane ($\epsilon = 5.02$ at 298 K).^[30] Electrolytes with high ionic conductivity can lower the internal resistance.^[6] The ionic conductivity of the three diglyme-based electrolyte systems at room temperature was 670, 1610 and 1700 $\mu S/cm$, respectively (Figure 1a). Scanning electron microscopy (SEM) images of the surface of a charged Mg anode after 200 cycles (Figure 1b) revealed the presence of Mg spheres approximately 150 nm in diameter. Only spherical but no dendritic structures were observed. The overpotential was measured by cycling symmetric Mg-Mg cells and proved high

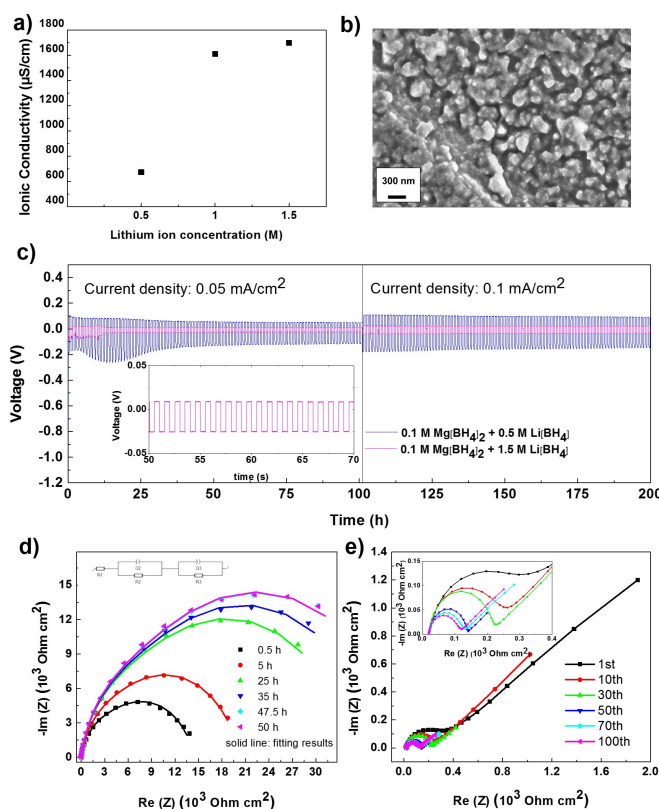


Figure 1. a) Ionic conductivity of the electrolytes: 0.1 M $Mg[BH_4]_2$ with 0.5 M, 1 M and 1.5 M of lithium ions in diglyme; b) SEM image of a Mg foil after long-term Mg plating and stripping test: no dendrite formation was observed within 200 cycles; c) long-term Mg plating and stripping over 200 cycles in 0.1 M $Mg[BH_4]_2/0.5$ M $Li[BH_4]$ /diglyme, and 0.1 M $Mg[BH_4]_2/1.5$ M $Li[BH_4]$ /diglyme at a current density of 0.05 and 0.1 mA/cm^2 , respectively, using symmetric Mg-Mg cells. Measurements were started directly after assembling the cells; d) Nyquist plots of a symmetric Mg-Mg cell containing 0.1 M $Mg[BH_4]_2/1.5$ M $Li[BH_4]$ /diglyme with resting times between 0.5 and 50 hours at OCV; e) Nyquist plots of a symmetric Mg-Mg cell containing 0.1 M $Mg[BH_4]_2/1.5$ M $Li[BH_4]$ /diglyme after the given number of cycles. Mg foils were applied in the measurements.

efficiency of the electrolyte. Thus, cells containing 0.1 M $Mg[BH_4]_2/1.5$ M $Li[BH_4]$ (Figure 1c pink, left) showed good cycle stability with a very low overpotential < 0.04 V at a current density of 0.05 mA/cm^2 for 100 hours. The inset of the voltage profile shows a rectangular potential profile, indicating smooth Mg plating and stripping. In comparison, cells containing 0.1 M $Mg[BH_4]_2/0.5$ M $Li[BH_4]$ showed a higher polarization potential up to 0.13 V (Figure 1c blue, left) indicating poorer Mg plating and stripping performance. It is worth to point out that the overpotential of the 0.1 M $Mg[BH_4]_2/1.5$ M $Li[BH_4]$ electrolyte is substantially lower than the one reported for the $Mg[B(hfp)_4]_2$ system (around 0.1 V).^[20]

2.2. Electrochemical Impedance Spectroscopy

Since the overpotential of a symmetric Mg-Mg cell based on 0.1 M $Mg[BH_4]_2/1.5$ M $Li[BH_4]$ up to cycle fifteen was higher than during the following 185 cycles (0.08 V vs. 0.04 V), electrochemical impedance spectroscopy (EIS) was applied,

both during open circuit voltage (OCV) and after cycling. Figure 1d shows the Nyquist plot of a resting symmetrical Mg–Mg cell at OCV (dots). The plot was fitted according to the model shown in the inset, comprising the high frequency resistance (R_1) and two RC (resistor and capacitor in parallel) elements in series. The two RC elements model the charge transfer reaction (R_2 and Q_2) and most likely a blocking layer on the anode (R_3 and Q_3).

Since the charge transfer resistance is several orders of magnitude higher than other resistance contributions,^[31–32] only one clear semicircle is visible and a distinction between the two resistances is not possible. For the following discussions, the sum of R_2 and R_3 will be described as the overall charge transfer resistance. Fits are shown as solid lines. For more clarity, the high frequency resistance (R_1) was subtracted from all measurements. The exact values of the resistance can be found in Table S1 in the Supporting Information. Impedance measurements clearly show an increase in impedance with increasing resting time of the cell at OCV. Impedance became constant after 47.5 hours, indicating a stabilization of the interface or fully wetting of the electrodes. Nonetheless, impedance decreased dramatically after cycling the cell, as shown in Figure 1e. These data can be interpreted in that some ion-blocking layer partially blocks the interface between the electrolyte and the Mg surface during resting the cell at OCV. However, after cycling, fresh and highly conductive Mg metal surfaces are reformed, leading to the pronounced drop in impedance. Similar observations, though with different electrolyte systems, have been reported by Oscar et al.^[33] and Zhao-Karger et al.^[6] and appear to be quite unique for Mg systems.

2.3. Electrochemical Characterization

Figure 2a shows that the cells with 0.1 M $\text{Mg}[\text{BH}_4]_2/0.5 \text{ M Li}[\text{BH}_4]$ (lower blue) and 0.1 M $\text{Mg}[\text{BH}_4]_2/1.5 \text{ M Li}[\text{BH}_4]$ in diglyme (lower red) deliver a discharge capacity of ca. 420 and 800 $\text{mAh/g}_{\text{sulfur}}$ at 0.1 C, respectively, both with virtually >99.8% Coulombic efficiency (Figure 2a top). In addition, the use of a coin cell setup with a reduced amount of electrolyte results in a virtually identical electrochemical performance (Figure S1 in the Supporting Information). This strongly indicates the high stability of the system and renders extensive sacrificial consumption of the electrolyte unlikely. The electrochemical performance of cells based on a 1 M $\text{Li}[\text{BH}_4]$ electrolyte was also measured (Figure S2). Performance of cells based on 1 M and 1.5 M $\text{Li}[\text{BH}_4]$, respectively, was very similar. Nonetheless, for further studies, the electrolyte with the highest lithium salt concentration (1.5 M) was used in order to prevent the potential dissolution of polysulfides.^[2] The rate tests in Figure 2b show the capacities fully recovered once the current rate was decreased, indicating good rate capability. For Coulombic efficiency see, Figure S3. The better performance of cells containing higher concentration of $\text{Li}[\text{BH}_4]$ are attributable to the higher ionic conductivity of the electrolyte (Figure 1a), which results in higher ion mobility. The capacity contributed by the potential intercalation of Li^+ or Mg^{2+} ions into the

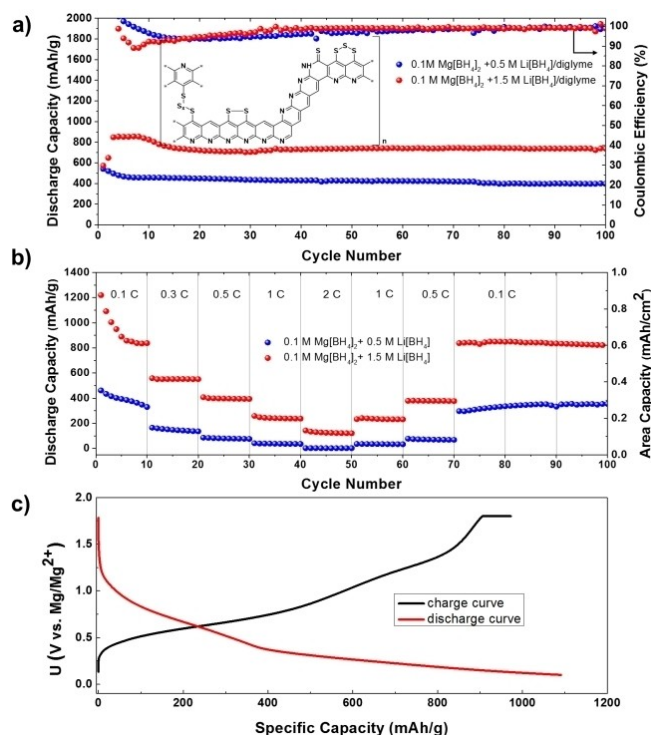


Figure 2. a) Long-term cycle stability of SPAN–Mg cells at 0.1 C, 22 °C, inset: structural features of SPAN, where $2 \leq x < 8$;^[34] b) rate test between 0.1 C and 2 C, 28 °C. All cells contained 0.1 M $\text{Mg}[\text{BH}_4]_2/0.5 \text{ M Li}[\text{BH}_4]$ and 0.1 M $\text{Mg}[\text{BH}_4]_2/1.5 \text{ M Li}[\text{BH}_4]$ in diglyme, respectively. The sulfur content of all cathodes was 0.6 mg/cm^2 ; c) typical discharge and charge profiles at 0.1 C of a cell containing 0.1 M $\text{Mg}[\text{BH}_4]_2/1.5 \text{ M Li}[\text{BH}_4]$ in diglyme.

graphite current collector was determined for an SPAN-free system consisting of a Mg foil, a graphite current collector and 0.1 M $\text{Mg}[\text{BH}_4]_2/1.5 \text{ M Li}[\text{BH}_4]$ in diglyme; only a minor contribution of 0.04 mAh/cm^2 was found (Figure S4). The charge and discharge voltage profiles (Figure 2c) as well as cyclic voltammetry (CV) measurements (Figure S5) of a Mg foil–SPAN cell using the 0.1 M $\text{Mg}[\text{BH}_4]_2/1.5 \text{ M Li}[\text{BH}_4]$ electrolyte provide some insight into the chemical reactions inside the cell. The first striking feature is that the voltage plateau around 1.5 V, which corresponds to the formation of long-chain polysulfides (e.g. MgS_8), is not observed.^[20] Similar was observed in Li–SPAN cells, in which only LiS_x species with $1 \leq x \leq 4$ were identified.^[24] This is attributed to the unique structure of SPAN that does not possess any elemental sulfur but only chemically bound sulfur chains (Figure 2a inset). Since the sulfur chain length in the SPAN structure has an upper limit of eight ($x \leq 6$) and the C–S bond is hard to break, no long-chain polysulfides, such as MgS_8 are formed with SPAN cathodes. Indeed, elemental analysis of the SPAN-based cathode of fully discharged Mg–SPAN cells contain ca. 11 wt-% of S and show an atomic ratio of N:S close to unity (0.98). This clearly indicates that the final C–S bonds in the SPAN structure are not broken even after full discharge. This is in line with a recent paper by Wang et al. on Li–S batteries.^[35] Instead, in the discharge curve, two distinct sloped regions were observed, one at 1.2–0.4 V and a second at 0.4–0.1 V. The first region is most probably attributable to the

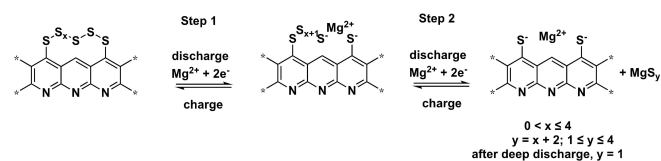
formation of magnesium polysulfides, such as MgS_4 or Mg_3S_8 .^[36] Scheme 1 outlines the proposed redox process of the SPAN cathode. After incorporation of Mg ions into the SPAN structure (step 1), MgS_4 and Mg_3S_8 , respectively, are proposed to form (Scheme 1, step 2). During further discharge, the sulfur species are released via breakage of the S–S but not of the C–S bond, due to the higher bonding energy of C–S bonds (Scheme 1, $y = 4$ or $8/3$). Since the potential of Li is similar to that of Mg, some Li polysulfides might also coexist inside the electrolyte. The second region of the discharge curve starts at around 0.4 V, which is the deep discharge of the system. This region indicates the formation of low-order magnesium sulfides, i.e., MgS and MgS_2 . MgS is stable and crystalline and therefore hard to re-oxidize to amorphous Mg_3S_8 and eventually also passivates the Mg anode.

Due to the existence of Li^+ ions inside of the system, however, some lithiation of the MgS is proposed to happen in this voltage range, which might also contribute to the overall capacity.^[4,36–38] The charge curve shows an almost constant increase from 0.4 to 1.8 V, suggesting multiple reactions in this voltage range. In the presence of Li^+ ions, (lithiated) MgS or MgS_2 react reversibly back to the polysulfides, such as Mg_3S_8 , contributing to the observed high reversibility. Overall, by integrating the discharge curve, an energy density of ca. 430 mWh/g_{sulfur} or 14 mWh/g_{cathode} at 0.1 C is obtained.

2.4. XPS Post-Mortem Analysis

To gain an insight of the sulfur species forming on the electrodes, ex situ high resolution X-ray photoelectron spectroscopy (XPS) was conducted on the pristine SPAN powder, as well as on anodes and cathodes fully charged and deep discharged over seven cycles. The sulfur-containing fragments S–S/S–C and S=C featured by the S $2p_{3/2}$ and S $2p_{1/2}$ signals in SPAN are shown in Figure 3a.

In particular the S $2p_{3/2}$ signals were used to monitor variations in the sulfur species during cycling.^[18,20] On the pristine SPAN powder, the S $2p_{3/2}$ signals at 161.7 and 163.4 eV are attributable to the S=C and C–S/S–S bonds.^[29] It should be noted that the pristine SPAN powder was pressed onto indium foil whereas the cycled SPAN was mixed with carbon black and coated onto a graphite current collector. This leads to a shift in binding energy compared to the pristine SPAN powder. After seven cycles, at a deep discharged state (0.1 V), the signal at 161.7 eV appears to be more pronounced than the one at 163.4 eV, suggesting that large amounts of lithium/magnesium



Scheme 1. Proposed redox process of the SPAN cathode. For simplicity, Mg^{2+} ions were used as model ion; MgS_y could transform to short sulfides ($y = 1, 2$). In the deep discharge state, it is in the form of MgS.

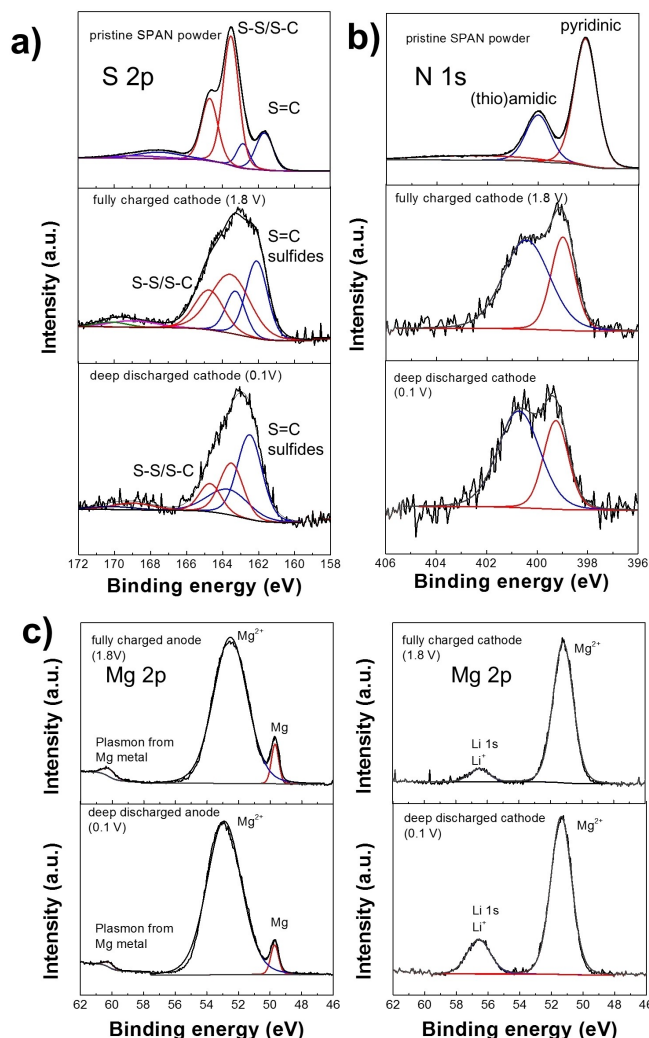


Figure 3. a) High-resolution S $2p$ (upper left) and b) N $1s$ (upper right) ex situ XPS spectra of pristine SPAN powder and aged cathodes and anodes after seven cycles at the fully charged and deep-discharged state, respectively. The pristine SPAN powder was pressed onto indium foil whereas the cycled SPAN was mixed with carbon black and coated onto graphite foil, which is partially conductive, resulting in the broader peaks of the cycled cathodes and the shift in binding energy compared to the pristine SPAN powder; c) Mg $2p$ (down) ex situ XPS spectra of pristine SPAN powder and aged cathodes and anodes after seven cycles at the fully charged and deep-discharged state, respectively.

sulfides are formed at 0.1 V on the cathode side, which is in line with the above-proposed redox process. Notably, after seven cycles and in the fully charged state (1.8 V), the detected peak positions are similar to those in pristine SPAN, in which the sulfur exists in the form of S=C, S–S and S–C species.^[35] This suggests that the SPAN framework as such is stable over the entire redox process. Further on, N $1s$ spectra of both pristine SPAN powder and aged cathodes (Figure 3b) suggest that the main features of SPAN structure including (thio)amidic (401.5 eV) and pyridinic (399.1 eV) chemical units are stable over the entire redox process. Figure 3c shows high resolution XPS spectra in the energy region of the Mg $2p$ and Li $1s$ core levels of aged electrodes after seven cycles at different voltage states. The spectrum of the Mg anode at a fully charged state

(1.8 V) shows a signal at 51.5 eV and a smaller one at 48.5 eV, which is assignable to Mg^{2+} (MgO , MgS or $\text{Mg}[\text{BH}_4]_2$) and Mg (0), respectively. Also, a small signal at 59.2 eV associated with the plasmon excitation of the magnesium nanoparticles might indicate the presence of plated Mg on the surface.^[39] In view of the redox potentials of Li (-3.04 V) and Mg (-2.36 V) and the maximum charging voltage of 1.8 V, the formation of Li (0) seems highly unlikely. On the cathode side, both samples (0.1 V and 1.8 V) contain substantial amounts of Li^+ observed at 56.1 eV. During discharge, more lithium polysulfide species are formed on the cathode, resulting in a more pronounced signal of the Li 1s peak at the discharged cathode. The Li species on the cathode at the charged state might stem from the electrolyte, lithium oxide and/or residual lithium polysulfides.

2.5. Role of the Mg Anodes

Apart from the cathode and the electrolyte, the anode plays a crucial role in electrochemical performance.^[40–42] Generally, a large specific surface area is highly desired since this offers a large number of sites for plating and stripping, thereby impeding the build-up of a passivation layer at the anode and reducing the resistance for charge transfer. In order to determine the influence of specific surface area on electrochemical performance, three different anode materials, i.e., Rieke Mg, commercial Mg powder and Mg foil, were used. Scanning electron micrographs show the plate-shaped particles of Rieke Mg, which were 30–50 nm thick and had a diameter of 0.3–2 μm (Figure 4a), while commercial Mg powder (Figure S6) consisted of substantially larger particles, typically 44 μm in diameter. The X-ray diffraction (XRD) spectrum of Rieke Mg powder shows the expected signals (Figure S7). N_2 -adsorption measurements (BET method) revealed a specific surface area of 13.43 m^2/g for Rieke Mg, which is more than one order of magnitude higher than the one of conventional Mg powder (325 mesh, 0.60 m^2/g). In sharp contrast, the surface area of Mg

foil was only 0.002 m^2/g and thus almost 7000 times smaller than the one of Rieke Mg. To investigate the effect of the specific surface area of the anode on electrochemical behavior, Mg anodes were prepared from Rieke Mg applying different pressures. According to Figure 4b–d, the surface gets smoother with increasing pressure. For the lowest pressure (13.8 MPa), the surface shows rough features with holes between the individual powder particles. Some cavities even form deep channels, where the individual particles can still be detected. This creates a larger surface area compared to a regular metal foil. The higher the pressure applied, the more cavities are closed. This occurs even at a low pressure of 55.1 MPa, while the surface of the Mg anode prepared 96.5 MPa is even flatter. N_2 -adsorption measurements (BET method) of the anodes prepared with different pressures support this trend.

Thus, the parent Mg powder had a specific surface area of 13.4 m^2/g , while anodes prepared at 13.8, 55.1 and 96.5 MPa had specific surface areas of 11.3, 11.6 and 9.4 m^2/g , respectively (Figure S8). However, it is important to note that the pellets had to be divided into two parts prior to measurements. This inevitably induces some error to all the measurements, especially for pellets prepared at high pressures, since the newly created cross-section area adds to the original surface area.

To study the impedance of the Mg powder anodes prepared at different pressures, symmetrical Mg–Mg cells were measured at OCV. Similar to the measurement presented in Figure 1d, a time-dependent increase of the impedance was also detected for the pressed anodes. For a more lucid comparison between the different types of anodes, only the impedance after resting for 1 hour at OCV is presented in Figure 5a. The Nyquist plots were fitted as described in Figure 1d; the exact fitting data are given in Table S2. Obviously, the impedance of all pressed Mg powder anodes is one order of magnitude lower than that of the foil. The inset shows a higher resolution of the curves of the pressed anodes. Clearly, impedance increased with increasing pressure during anode preparation. The charge transfer resistances were 331, 773 and 1150 Ω for the Mg anodes prepared at 13.8, 55.1 and 96.5 MPa, respectively. This clearly indicates that the higher the surface area of the anode is, the lower the resistance for the charge transfer of the Mg^{2+} becomes. Notably, the charge transfer resistance did not linearly increase with increasing preparation pressure. Instead, a more pronounced increase of the impedance between the anodes prepared at 13.8 and 55.1 MPa, compared to the impedance increase between the 55.1 and 96.5 MPa, was found. This can be explained by SEM: at pressures higher than 13.8 MPa, the individual particles progressively fuse together, resulting in a much smaller surface area. Notably, this is to the best of our knowledge the first correlation between anode morphology and the charge transfer resistance reported so far.

To determine the influence of the different charge transfer resistance on cycle stability, the electrochemical performance of Mg–S cells prepared from pressed Mg-anodes fabricated at different pressures was studied applying a discharge rate of 0.5 C. Results are shown in Figure 5b.

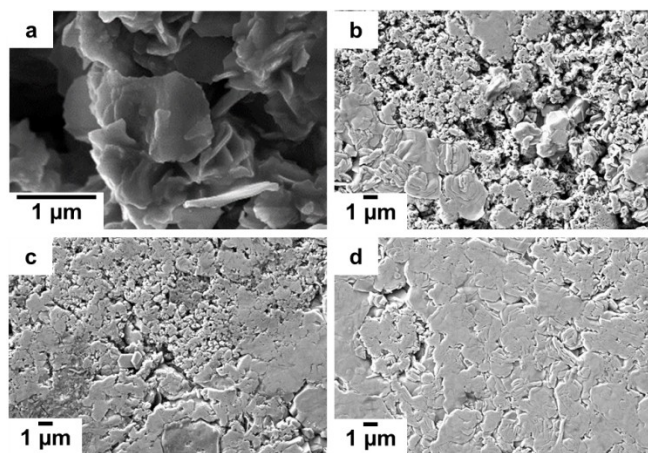


Figure 4. SEM images of the surfaces of pressed anodes prepared from Rieke Mg with different preparation pressures: a) pristine Rieke Mg powder, b) 13.8 MPa, c) 55.1 MPa, d) 96.5 MPa.

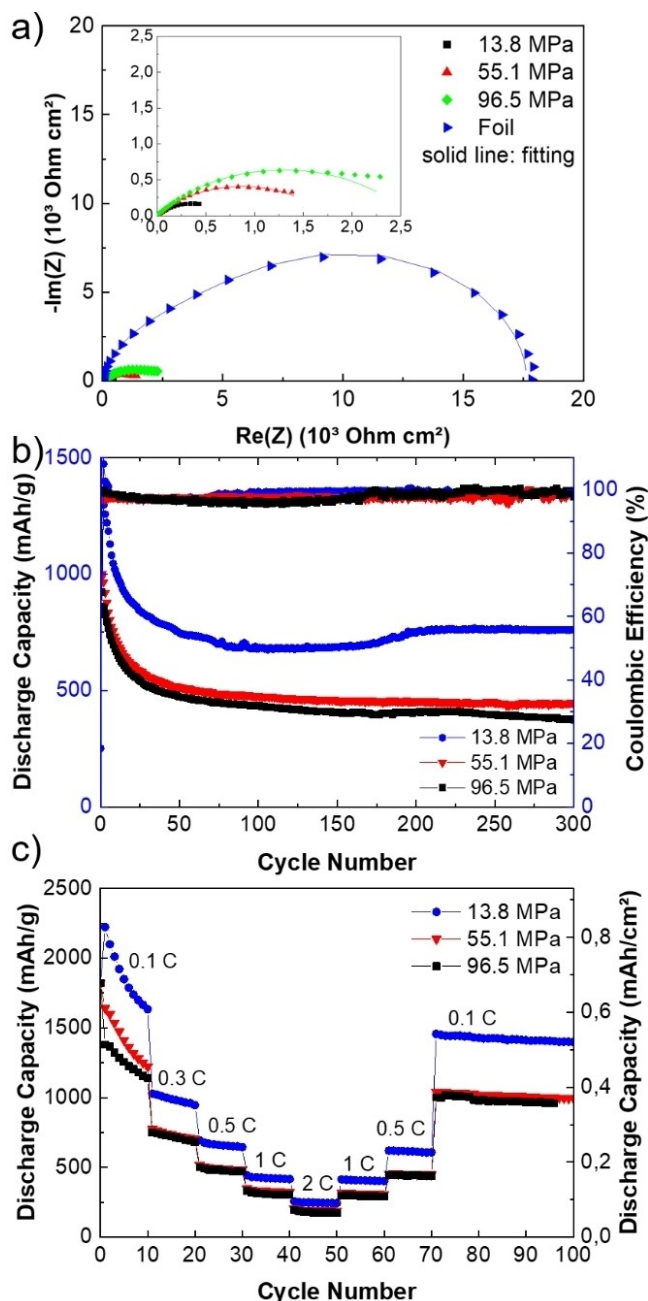


Figure 5. a) Nyquist plots of a symmetric Mg–Mg cell containing 0.1 M Mg [BH₄]₂/1.5 M Li[BH₄]₂/diglyme after 1 hour resting time at OCV with Mg anodes prepared from Rieke Mg at different pressure and from a Mg foil for comparison. Inset: Enlarged part of the plot showing only the impedance of the powder anodes and the equivalent circuit for fitting. b) Long-term cycle stability of SPAN–Mg cells with pressed Mg anode at 0.5 C, 22 °C; c) rate tests between 0.1 C and 2 C, 22 °C. All cells contained 0.1 M Mg[BH₄]₂/1.5 M Li [BH₄]₂/diglyme.

The Coulombic efficiency remained constant at ca. 100%, suggesting that the system is stable. On top of that, a higher cycle stability than with cells based on a Mg-foil was observed: more than 300 cycles could be run without any signs of decomposition. For all pressed anodes, the discharge capacity was higher compared to the foil anode. Cells containing anodes compacted with the lowest pressure (13.8 MPa) show discharge

capacities of ca. 800 mAh/g_{sulfur} at 0.5 C. With increasing fabrication pressure of the anodes, decreasing capacities were observed, though still with good cycle stability. In line with the results for charge transfer resistance and with the observations from SEM, the differences in capacity became less pronounced with increasing fabrication pressure. In addition, the difference in capacity for the differently prepared anodes become smaller at higher C-rates (Figure 5c). Cells containing a Mg-anode prepared at 13.8 MPa delivered 1400 mAh/g_{sulfur} at 0.1 C, and 250 mAh/g_{sulfur} at 2 C. Notably, upon cycling between 0.1 C and 2 C, capacity reestablishes to 1500 mAh/g_{sulfur} after 70 cycles when returning to 0.1 C for a cathode prepared at 13.8 MPa.

Differences in capacity between a cell containing a Mg-anode prepared at 13.8 MPa and one prepared at 96.5 MPa were 400 mAh/g_{sulfur} and 70 mAh/g_{sulfur} at 0.1 C and 2 C, respectively. The Coulombic efficiency for the rate test was ca. 100% for every tested C-rate (Figure S9). These observations clearly reveal the importance of anode morphology and specific surface area to allow a fast and reversible Mg plating. Similar to what was found for the Mg-foil, the capacity contributed by any possible Li-ion intercalation into the graphite current collector was negligible, as can be deduced from Figure S10.

Finally, it is worth to mention that the charge and discharge voltage profiles of cells based on SPAN and pressed Mg anodes (Figure S11) were similar as those obtained with cells based on SPAN and a standard Mg foil anode, confirming that the same electrochemical reactions occur during cycling. By integrating the discharge curve, a power density of ca. 400 mWh/g_{sulfur} or 13 mWh/g_{cathode} though at a discharge rate of 0.5 C, was determined. A summary of the electrochemical performance of the different anodes is given in Table S3.

3. Conclusions

The first long-lasting Mg–SPAN cell based on a Mg[BH₄]₂/Li[BH₄]₂ electrolyte in diglyme has been developed. The tailored electrolyte features a low overpotential of only 0.04 V and efficiently removes any blocking layer on the surface of the Mg foil. SPAN-based Mg–S cells based on the novel electrolyte deliver around 800 mAh/g_{sulfur} at 0.1 C and also show very good rate capability. Compared to Mg foils, the utilization of the pressed Rieke Mg anodes further improves cell performance, allowing for ca. 800 mAh/g_{sulfur} at 0.5 C over 300 cycles. Post-mortem analysis supports the proposed redox mechanism of the SPAN cathodes. In summary, the combination of SPAN as cathode material with this particular “dual” electrolyte and high surface area Mg anodes clearly offers new opportunities for Mg–S cells.

Experimental Section

Chemicals

All samples were handled in an Ar-filled glove box with water and oxygen levels < 0.1 ppm. All glassware was dried in an oven at 120 °C. Mg(BH₄)₂ (95%), Li[BH₄] (> 95%) PAN (*M_n* = 36,500 g/mol, *D* = 3.6), MgCl₂, naphthalene and anhydrous diethyleneglycol dimethyl ether (diglyme, 99.5%, anhydrous) were purchased from Merck and used as received. Li foils were purchased from Alfa Aesar and were polished before use. Mg foil (0.25 mm thick, 99.9%) and graphite foil (0.13 mm, 99.8%) were purchased from Alfa Aesar Germany. The Mg chips were polished with a ceramic knife inside a glovebox to remove the oxide layer before assembling the cells.

Preparation of Mg[BH₄]₂/Li[BH₄] solutions in diglyme

In an argon-filled glovebox, 21.6 mg Mg[BH₄]₂ (0.1000 mol) and 132 mg Li[BH₄] (1.500 mol) were dissolved in 4 mL diglyme. The mixture was stirred at room temperature overnight, then filtered through a glass fiber filter and stored over molecular sieves for at least one day in the glovebox. The preparation of 0.1 M Mg[BH₄]₂/1 M Li[BH₄] and 0.1 M Mg[BH₄]₂/0.5 M Li[BH₄] solutions in diglyme was conducted in the similar way. The ¹H NMR spectrum of the electrolyte can be found in Figure S12. The ionic conductivity of the electrolyte solutions with different concentrations was measured using an InLab Sensor conductometer (Mettler Toledo).

Preparation of SPAN

The active material in the cathode, sulfurated poly(acrylonitrile) (SPAN) was prepared via a two-step reaction. First, 1.00 g of poly(acrylonitrile) (PAN) powder was thoroughly mixed with excess (ca. 15 g) sulfur powder inside a high-temperature resistant quartz glass tube, which was heated to 150 °C under Ar. After the sulfur in the glass tube was fully molten, the tube was cooled to room temperature and placed inside a furnace apparatus. The temperature of the oven was first increased to 150 °C within 30 minutes and then held for 30 minutes. Then, the temperature was gradually increased to 550 °C over 3 hours and held for another 5 hours. The oven was allowed to cool to room temperature overnight and the quartz glass tube was removed from the oven. Then, a heat gun was used to melt and remove the obtained SPAN (black) with excess sulfur (yellow). After that, in order to remove excess sulfur, the material was extracted in a Soxhlet apparatus using hot toluene for 2 days until no further sulfur could be extracted. The obtained SPAN compound was further dried in vacuo overnight and then manually ground with the aid of a mortar and a pestle in order to reduce the particle size of the SPAN particles. To achieve a more homogeneous particle size distribution, the SPAN particles were sieved by a 63 μm sieve. Elemental analysis of SPAN: C, 44.08%; H, 1.048%; N, 13.66%; S, 38.32%.

Preparation of the cathodes

For preparing the coated cathodes, the weight ratio of SPAN: carbon black: binder was set to 70:15:15. The weight ratio of N-methyl-2-pyrrolidone (NMP): SPAN was set to 10:1. The dispersion of the SPAN, the conductive material, the binder and NMP was thoroughly mixed at 20,000 rpm for 6 minutes. Then the slurry was coated on a graphite foil. The wet coating was dried on a vacuum plate at 60 °C and under air suction for several hours. After the coating was nearly dry, it was transferred to an oven at 60 °C for further drying. Then, round chips 12 mm in diameter were punched out. The average sulfur content was around 0.6 mg/cm²

per cathode, corresponding to 1.0 mAh/cm². The binder used for all measurements was poly(vinylidene difluoride) (PVDF), except for cathodes subjected to post-mortem elemental analysis; for these, poly(acrylic acid) (PAA) was used.

Preparation of pressed anodes

Rieke Mg was synthesized by the reduction of MgCl₂ with Li and naphthalene as an electron carrier.^[27] All chemicals were dried prior to use and the procedure was conducted in an Ar-filled glovebox. Naphthalene (27.7 g, 216 mmol) was dissolved in 150 mL of dry THF. To this solution, freshly polished Li (1.5 g, 216 mmol) was added in pieces. MgCl₂ (10.3 mg, 108 mmol) was added slowly to keep the exothermic reduction under control. After vigorous stirring for at least 15 h, the precipitated Mg powder was washed several times with THF and diethyl ether. The XRD pattern of the synthesized Mg powder is shown in Figure S7. The synthesized powder was then pressed with the aid of a hydraulic press in an argon filled glovebox, applying 13.8, 55.1 and 96.5 MPa, respectively.

Electrochemistry

Cells were assembled in an Ar-filled glovebox. Both the over-potential and the long-term cycle stability were tested using symmetric Mg–Mg Swagelok-type cells using two pieces of Mg foils containing the corresponding electrolyte. Discharging and charging of the cells was performed at a constant current for 0.5 h at 0.05 and 0.1 mA/cm², respectively.

For testing cycle stability and for investigating the influence of different concentrations of the [BH₄][−] anion in the electrolytes, Swagelok cells were built from an SPAN cathode and Mg foil using 0.1 M Mg[BH₄]₂ and 1.5 M Li[BH₄]/0.5 M Li[BH₄] dissolved in diglyme as electrolyte. Cells comprised one Mg foil (12 mm diameter), one SPAN cathode (12 mm diameter) and two Whatman glass fiber separators. 100 μL of electrolyte were added onto each of the separators. The Mg foil was thoroughly scratched with a ceramic knife inside a glovebox to remove the oxide layer. For comparison, coin cells using the same system were manufactured using 130 μL of electrolyte. All cycling data were recorded on a BasyTec XCTS-LAB system. Cells were cycled at a potential window of 0.1–1.8 V to avoid decomposition of the electrolyte at higher voltage.^[43] Long-term cycle stability testing was performed at 0.1 C at room temperature (22 °C) using two electrolytes with different concentrations. CV-measurements were conducted using a three-electrode cell set-up (PAT cell from EL-CELL ©) with SPAN as working electrode (WE), Mg foil as the counter and reference electrodes (Mg_{CE} and Mg_{RE}).

Rate capability testing of the cells was investigated using a stress test that comprised cycling ten times each at 0.1 C, 0.3 C, 0.5 C, 1 C, 2 C and then back to 0.1 C for another 30 cycles. (0.1 C = 0.1 mA/cm²).

Electrochemical impedance spectroscopy (EIS) data of the open circuit voltage (OCV) were measured with a signal amplitude of 10 mV in a frequency range from 300 kHz to 100 mHz with no current applied on Biologic VMP3. Data were fitted using the integrated EC-Lab software. The resistance data were normalized to the geometrical area of the electrode.

Measurement of the powder surface area by nitrogen adsorption

Nitrogen adsorption analyses were performed at 77 K on a Quantachrome Instruments Autosorb iQ MP automatic volumetric instrument. Magnesium samples were degassed for 16 hours at 150 °C under vacuum prior to the gas adsorption studies. Surface areas were evaluated using the eleven-point Brunauer-Emmett-Teller (BET) model implemented in the ASiQwin software version 3.01.

Ex situ XPS measurements

For ex situ XPS measurements, Mg–S cells were disconnected from the BasyTech after seven cycles. All cells were opened in an Ar-filled glovebox and the electrodes were thoroughly rinsed with DME and dried in vacuo overnight to remove all the solvent. The electrodes were then fixed on a sample holder and transferred under argon atmosphere directly into the X-ray photoelectron spectrometer to avoid any contamination with air. Pristine SPAN spectra were obtained by measuring pure SPAN powder stabilized on indium foil. XPS was performed on a Kratos Axis Ultra system equipped with a monochromatic Al K_α source using a pass-energy of 20 eV for the high-resolution measurements. Data were analyzed using CasaXPS. The energy separation and peak area of the S 2p_{3/2} and S 2p_{1/2} were constrained according to the literature.^[44] Broader peaks and spikes in the Mg 2p spectra were a result of the charging of the anodes. Characteristic C1s signals of SPAN were calibrated to 284.8 eV according to the literature.^[29]

Post-mortem analysis of the discharged cathodes

Mg–SPAN cells based on Mg foil anodes were disconnected at a fully discharged state (0.1 V) after two cycles. The cathodes were thoroughly washed with DME and dried. The coating was then removed from the graphite current collector. Elemental analysis of the obtained powder revealed 4.75 wt% N and 11.12 wt% S, respectively. The corresponding molar ratio of N to S was ca. 0.98.

Acknowledgements

Financial support by the German Federal Ministry of Education and research (project number 03XP0208J) and by the German Federal Ministry of Economic Affairs and Energy (project number 03ETE003E) is gratefully acknowledged. The authors would also like to thank the Ministry of Science, research and Arts of the Federal State of Baden-Württemberg for the financial support of the projects within the InnovationsCampus Mobilität der Zukunft. Finally, we wish to thank Mr. U. Hageroth from the German Institutes of Textile and Fiber Research (DITF) Denkendorf and Mr. B. Fenk from the Max Planck Institute for Solid State Research, Stuttgart, for the SEM measurements. Open access funding enabled and organized by Projekt DEAL.

Conflict of Interest

The authors declare no conflict of interest.

Keywords: magnesium · sulfur · sulfurized polyacrylonitrile · SPAN · borohydride · batteries

- [1] H. Kim, T. S. Arthur, G. D. Allred, J. Zajicek, J. G. Newman, A. E. Rodnyansky, A. G. Oliver, W. C. Boggess, J. Muldoon, *Nat. Commun.* **2011**, *2*, 1–6.
- [2] P. Wang, M. R. Buchmeiser, *Adv. Funct. Mater.* **2019**, *29*, 1905248–1905275.
- [3] T. Gao, S. Hou, F. Wang, Z. Ma, X. Li, K. Xu, C. Wang, *Angew. Chem.* **2017**, *129*, 13711–13715; *Angew. Chem. Int. Ed.* **2017**, *13526–13530*.
- [4] S. Y. Ha, Y. W. Lee, S. W. Woo, B. Koo, J. S. Kim, J. Cho, K. T. Lee, N. S. Choi, *ACS Appl. Mater. Interfaces* **2014**, *6*, 4063–4073.
- [5] X. Ji, K. T. Lee, L. F. Nazar, *Nat. Mater.* **2009**, *8*, 500–506.
- [6] Z. Zhao-Karger, M. E. G. Bardaji, O. Fuhr, M. Fichtner, *J. Mater. Chem. A* **2017**, *5*, 10815–10820.
- [7] W. Li, S. Cheng, J. Wang, Y. Qiu, Z. Zheng, H. Lin, S. Nanda, Q. Ma, Y. Xu, F. Ye, M. Liu, L. Zhou, Y. Zhang, *Angew. Chem.* **2016**, *128*, 6516–6520; *Angew. Chem. Int. Ed.* **2016**, *55*, 6406–6410.
- [8] A. Du, Z. Zhang, H. Qu, Z. Cui, L. Qiao, L. Wang, J. Chai, T. Lu, S. Dong, T. Dong, H. Xu, X. Zhou, G. Cui, *Energy Environ. Sci.* **2017**, *10*, 2616–2625.
- [9] X. Yu, M. Arumugam, *ACS Energy Lett.* **2016**, *1*, 431–437.
- [10] P. Zuo, Y. Li, M. He, R. Li, Y. Ma, C. Du, Y. Gao, G. Yin (Harbin Institute of Technology), CN107910535A, **2018**.
- [11] T. Gao, M. Noked, A. J. Pearse, E. Gillette, X. Fan, Y. Zhu, C. Luo, L. Suo, M. A. Schroeder, K. Xu, S. B. Lee, G. W. Rubloff, C. Wang, *J. Am. Chem. Soc.* **2015**, *137*, 12388–12393.
- [12] A. C. Kozen, C. F. Lin, A. J. Pearse, M. A. Schroeder, X. Han, L. Hu, S. Lee, G. W. Rubloff, M. Noked, *ACS Nano.* **2015**, *9*, 5884–5892.
- [13] B. P. Vinayan, Z. Zhao-Karger, T. Diemant, V. S. Chakravadhanula, N. I. Schwarzburger, M. A. Cambaz, R. J. Behm, C. Kubel, M. Fichtner, *Nanoscale* **2016**, *8*, 3296–3306.
- [14] Y. Cheng, Y. Shao, J. G. Zhang, V. L. Sprenkle, J. Liu, G. Li, *Chem. Commun.* **2014**, *50*, 9644–9646.
- [15] Z. Zhao-Karger, X. Zhao, D. Wang, T. Diemant, R. J. Behm, M. Fichtner, *Adv. Energy Mater.* **2014**, *5*, 1401155–1401164.
- [16] C. Fotea, J. Callaway, M. R. Alexander, *Surf. Interface Anal.* **2006**, *38*, 1363–1371.
- [17] M. Santamaria, F. Di Quarto, S. Zanna, P. Marcus, *Electrochim. Acta* **2007**, *53*, 1314–1324.
- [18] Y. Xu, G. Zhou, S. Zhao, W. Li, F. Shi, J. Li, J. Feng, Y. Zhao, Y. Wu, J. Guo, Y. Cui, Y. Zhang, *Adv. Sci.* **2019**, *6*, 1800981–1800987.
- [19] L. Zeng, N. Wang, J. Yang, J. Wang, Y. Nuli, *J. Electrochem. Soc.* **2017**, *164*, A2504–A2512.
- [20] Z. Zhao-Karger, R. Liu, W. Dai, Z. Li, T. Diemant, B. P. Vinayan, C. Bonatto Minella, X. Yu, A. Manthiram, R. J. Behm, M. Ruben, M. Fichtner, *ACS Energy Lett.* **2018**, *3*, 2005–2013.
- [21] I. Shterenberg, M. Salama, H. D. Yoo, Y. Gofer, J.-B. Park, Y.-K. Sun, D. Aurbach, *J. Electrochem. Soc.* **2015**, *162*, A7118–A7128.
- [22] Y. Yang, W. Wang, Y. Nuli, J. Yang, J. Wang, *ACS Appl. Mater. Interfaces* **2019**, *11*, 9062–9072.
- [23] L. Wang, X. M. He, J. J. Li, M. Chen, J. Gao, C. Y. Jiang, *Electrochim. Acta* **2012**, *72*, 114–119.
- [24] J. Fanous, M. Wegner, M. B. M. Spera, M. R. Buchmeiser, *J. Electrochem. Soc.* **2013**, *160*, A1169–A1170.
- [25] J. Fanous, M. Wegner, J. Grimminger, M. Rolff, M. B. M. Spera, M. Tenzerb, M. R. Buchmeiser, *J. Mater. Chem.* **2012**, *22*, 23240–23245.
- [26] J. Fanous, M. Wegner, J. Grimminger, A. Andresen, M. R. Buchmeiser, *Chem. Mater.* **2011**, *23*, 5024–5028.
- [27] R. D. Rieke, *Science* **1989**, *246*, 1260–1264.
- [28] Y. Shao, T. Liu, G. Li, M. Gu, Z. Nie, M. Engelhard, J. Xiao, D. Lv, C. Wang, J. G. Zhang, J. Liu, *Sci. Rep.* **2013**, *3*, 1–7.
- [29] M. Frey, R. K. Zenn, S. Warneke, K. Müller, A. Hintennach, R. E. Dinnebier, M. R. Buchmeiser, *ACS Energy Lett.* **2017**, *2*, 595–604.
- [30] C. F. Riadigos, R. Iglesias, M. A. Rivas, T. P. Iglesias, *J. Chem. Thermodyn.* **2011**, *43*, 275–283.
- [31] B. T. Habte, F. Jiang, *Solid State Ionics* **2018**, *314*, 81–91.
- [32] B. Yan, M. Li, X. Li, Z. Bai, L. Dong, D. Li, *Electrochim. Acta* **2015**, *164*, 55–61.
- [33] O. Tutusaus, R. Mohtadi, N. Singh, T. S. Arthur, F. Mizuno, *ACS Energy Lett.* **2016**, *2*, 224–229.
- [34] S. Warneke, R. K. Zenn, T. Leberherz, K. Müller, A. Hintennach, U. Starke, R. E. Dinnebier, M. R. Buchmeiser, *Adv. Sustain. Syst.* **2018**, *2*, 1700144–1700149.

- [35] W. Wang, Z. Cao, G. A. Elia, Y. Wu, W. Wahyudi, E. Abou-Hamad, A.-H. Emwas, L. Cavallo, L.-J. Li, J. Ming, *ACS Energy Lett.* **2018**, *3*, 2899–2907.
- [36] Y. Xu, Y. Ye, S. Zhao, J. Feng, J. Li, H. Chen, A. Yang, F. Shi, L. Jia, Y. Wu, X. Yu, P. A. Glans-Suzuki, Y. Cui, J. Guo, Y. Zhang, *Nano Lett.* **2019**, *19*, 2928–2934.
- [37] M. Helen, M. Fichtner, *Electrochim. Acta* **2015**, *169*, 180–185.
- [38] M. Wang, X. Li, M. Gao, H. Pan, Y. Liu, *J. Alloys Compd.* **2014**, *603*, 158–166.
- [39] J. Chang, R. T. Haasch, J. Kim, T. Spila, P. V. Braun, A. A. Gewirth, R. G. Nuzzo, *ACS Appl. Mater. Interfaces* **2015**, *7*, 2494–2502.
- [40] P. Saha, M. K. Datta, O. I. Velikokhatnyi, A. Manivannan, D. Alman, P. N. Kumta, *Prog. Mater. Sci.* **2014**, *66*, 1–86.
- [41] H. D. Yoo, I. Shterenberg, Y. Gofer, G. Gershinsky, N. Pour, D. Aurbach, *Energy Environ. Sci.* **2013**, *6*, 2265–2279.
- [42] J. Song, E. Sahadeo, M. Noked, S. B. Lee, *J. Phys. Chem. Lett.* **2016**, *7*, 1736–1749.
- [43] F. Tuerxun, Y. Abulizi, Y. NuLi, S. Su, J. Yang, J. Wang, *J. Power Sources* **2015**, *276*, 255–261.
- [44] J. F. Moulder, W. F. Stickle, P. E. Sobol, K. D. Bomben, *Handbook of X-ray Photoelectron Spectroscopy*, Physical Electronics Division, Perkin-Elmer Corporation, Minnesota, **1992**, pp. 1–261.

Manuscript received: May 5, 2020
Revised manuscript received: July 3, 2020
Accepted manuscript online: July 3, 2020
Version of record online: July 22, 2020